4.1 Introduction

New biochemical sensor platforms have been introduced recently to improve the industry of biosensors and analytical performance, as a result of recent advancements in nanoscience and nanotechnology. There has been a lot of interest among researchers for the development of innovative electrochemical sensors that make use of the superior features of nanomaterials. Nanomaterials, particularly metal and metal oxide nanoparticles, have garnered significant interest for their effectiveness in various biological processes and reactions, due to their adaptable sizes and shapes [1]. In order to maintain cellular equilibrium, the human body secretes nicotinamide adenine dinucleotide (NAD), a product of vitamin B3. Dihydro-nicotinamide adenine dinucleotide (NADH) and nicotinamide adenine dinucleotide (NAD^+) is crucial charge-carrying cofactors that are required for the activity of several pivotal metabolic pathways, such as DNA repair, tricarboxylic acid cycle, glycolysis, oxidative phosphorylation, and cell signalling [2,3].

The components of NADH include an adenine, nicotinamide, two ribose rings, and two bridging phosphate groups. The complex structure makes it challenging to create the best probes for biological system detection [4]. The adenine derivatives, i.e., NADH and NAD^+ are widely recognized as the core conductors in living cells [5]. NADH plays a wide range of biological functions and is closely linked to a number of illnesses, including cancer, Alzheimer's, Parkinson's, insomnia, and melancholy. Therefore, an improvement of effective and affordable NADH detection techniques is needed in the areas of biochemistry [6,7]. In the past, numerous NADH measurement techniques, including spectroscopy, capillary electrophoresis, chromatography, high-performance liquid, and others, have been suggested [5,8,9]. These methods have shortcomings, though, like poor sensitivity, slow response time,

and a complex system, which make them unsuitable. Due to their straightforward operation, cheapness, and quick response, electrochemical sensors are a good solution for these issues [10,11]. Much attention has been given to the electrochemical detection of NADH. Numerous NADH-based biosensors have been created over time using various transducer components, including carbon nanotubes and transition metals, and noble metals [12,13]. According to several reports, more than 300 dehydrogenase enzymes depend on the NAD^+/NADH pairs as vital cofactors [14,15].

The electrochemical oxidation of NADH is very interesting because it is required as a cofactor in many dehydrogenase-based biosensors [16]. Numerous alternative electrode configurations, such as reduced graphene oxide (rGO) and graphene functionalized with ionic liquids, have been studied as NADH sensors. Large overpotentials (often > + 0.5 V) are required, which frequently results in electrode fouling from the adsorption of NAD^+ in its oxidized state [17]. Numerous biochemical events are driven by the cofactors NADH and NAD^+, and their ratio is a crucial metabolic indicator of cellular health. Traditional NADH/NAD^+ ratio measurements are labor-intensive, prone to error, and unsuitable for high throughput screening [18]. NADH is additionally utilized to increase dopamine synthesis in the treatment of Parkinson's disease. It has been shown that substrate enzymes can add to or remove chemicals from protein molecules in biological processes using either NADH or NAD^+ (oxidized form) [19]. The creation and stimulation of neurotransmitters like dopamine, serotonin, and noradrenaline in cells to enhance muscle action and cerebral focus is also a function of NADH [20].

Furthermore, at common solid electrodes like carbon, gold, and platinum electrodes the direct oxidation of NADH proceeds at a higher potential and is a highly irreversible process,

which may be brought on by slow kinetics at the electrode surface [21]. Such analysis would experience severe interference issues that would result in incorrect findings because the actual samples contain frequently occurring electroactive species like ascorbic acid and uric acid [22]. By precisely changing the electrode surface with an appropriate material, this issue can be solved. Nanostructures have been used to drastically alter electrochemical sensors in the last few years. Due to their unique electrical, magnetic, catalytic, and optical capabilities, which support redox processes and have a large specific surface area, metal nanoparticles (NPs) have drawn a great deal of interest among nanostructures [23]. Silver nanoparticles of different geometry, such as nanospheres, nano prisms, and nanorods, were utilized to construct a simple and accurate NADH sensor [24]. The noble metal palladium (Pd), which has a number of intriguing qualities, including electrocatalysis activity and strong heterogeneous catalysis, adaptability, non-toxicity, and a comparatively low budget [25].

It has a broad range of applications in the area of analytical electrochemistry. Palladium nanoparticles (PdNPs) decorated electrostatically functionalized multi-walled carbon nanotubes served as a non-enzymatic glucose sensor, while electrochemical co-deposition of Pd and glucose oxidase enzymes onto nafion-solubilized carbon nanotube film was used as a glucose bio-sensor. Both methods demonstrated strong electrocatalytic activity to produce a low detection limit for nitrite determination [25–27]. Here, we have synthesized a novel composite (Co-NC/Pd), Pd was adsorbed on ordered Co-N doped carbon (NC) in the current study.

4.2 Experimental

4.2.1 Materials The following items were purchased from Sigma Aldrich- dimethyl ferrocene (Dmfc), graphite powder (particle size 20 ≤ µm), K_2PdCl_4, nitrilotriacetic acid (NTA), NADH, Nujol oil (density 0.838 g/ml), and Cobalt chloride hexahydrate. Himedia Chemicals in India provided the anhydrous disodium hydrogen phosphate (Na_2HPO_4), and dihydrogen sodium phosphate monohydrates ($NaH_2PO_4.H_2O$). We bought 3-APTMS from TCI India. All chemicals utilized were of analytical grade and were used without further purification.

4.2.2 Fabrication of Co-NTA Precursor

Co-NTA has been synthesized by using the hydrothermal method in the Teflon line autoclave in an oven at 120 °C for 8 h. 250 mg of $CoCl_2.6H_2O$ was dissolved in 15 mL deionized water and agitated for 20 min to form a homogeneous solution. 200 mg of NTA was distributed and swirled for 10 min in 15 mL of 2-propanol. The NTA solution was mixed to the cobalt chloride solution and agitated for 20 min. It was essential to let the autoclave drop to ambient temperature. The pink precipitate was collected, washed with deionized water several times, and then centrifuged with ethanol at 7000 rpm for 5 min. The recovered solid was dried for 6 h in a hot air oven set to 60 °C [28].

4.2.3 Synthesis of Co-NC/Pd

The use of NTA as a chelating agent has been well documented, and it may aid in the production of a one-step cobalt NTA complex, which is a prerequisite to the development of Co-NC, i.e., N-doped carbon that is the most suitable for the controlled doping of

organotrifunctionalized palladium nanoparticles. Consequently, the first step is to create the Co-NTA, which has been utilized to create Co-NC/Pd.

4.2.4 Measurements and Characterizations

XRD (The Rigaku Miniflex-600) pattern with Cu Kα radiation (λ= 0.154 nm), X-ray photoelectron spectroscopy, Transmission electron microscope (Tecnai G2 20 TWIN, FEI Electron Optics), and High-Resolution Scanning electron Microscope (HR-SEM, Nova Nano SEM-450) were used to characterize the morphology and crystal structure of the obtained catalyst.

4.2.5 Fabrication of Co-NC/Pd modified carbon paste electrode

Pd nanoparticles colloidal solution was synthesized through a wet chemical reduction process using 3-APTMS (10 mM and 5.4 M), with a slight modification based on a previously reported method [11] . Briefly, 160 µl of a 20 mM ethylene glycol solution of K_2PdCl_4 was mixed with 10–20 µl of a 10 mM 3-APTMS solution in a microcentrifuge tube, followed by the addition of 20 µl of a 1% ethanolic PVP solution. The resultant was mixed on a cyclo mixture and stirred for 3 to 5 min, and incubated in a microwave oven for 40 to 50 s, the obtained black color colloidal solution, was absorbed by as-prepared Co-NTA precursors. This prepared residue was calcined in a nitrogen environment in a tube furnace at 600 °C. The obtained material is represented as Co-NC/Pd. The solid residues (Co-NC/Pd and Graphite) were thoroughly mixed with Dmfc in a mortar and pestle. The presence or absence of Co-NC/Pd in the active paste led to the production of modified carbon paste electrode (CPE) systems such as CPE/Dmfc, CPE/Dmfc/Co-NC, and CPE/Dmfc-Co-NC/Pd. The borosilicate glass capillaries were used for the fabrication of a carbon paste electrode body. The well of the

electrode body was filled with a modified carbon paste containing the ingredients shown in **Table 4.1**.

Table 4.1 Composition of the mediator-modified electrode

System	Dmfc (w/w%)	Co-NC/Co-NC/Pd mixed with graphite(w/w%)	Graphite (w/w%)	Nujol oil (w/w%)
Dmfc/CPE	2.0	-	68.0	30
Dmfc-Co-NC/CPE	2.0	2	66.0	30
Dmfc-Co-NC-Pd/CPE	2.0	2	66.0	30

4.2.6 Electrochemical Measurement

The electrochemical experiments were recorded using a computer-controlled electrochemical workstation Model CHI 660B TX, USA. Using an experimental set-up where the resistance was gradually compensated for the uncompensated state, each CV was recorded many times. Using a three-electrode cell setup with a working capacity of 3 ml, the measurements were performed. An Ag/AgCl electrode (RE1B, ALS Co. Japan) and a Pt foil electrode are used as reference and counter electrodes. All potentials given below were relative to the Ag/AgCl. The modified carbon paste electrode was used as a working electrode. NADH was detected using cyclic voltammetry (CV), and amperometry i-t curve study. The phosphate buffer solution (PBS, 0.1 M, pH 7.0) containing 0.5 M KCl as supporting electrolyte was used as working electrolyte. The electrochemical impedance measurements were performed using a potentiostat/galvanostat (CHI 660B) over a frequency range of 100 kHz to 10 Hz. Freshly

prepared NADH was used for all experiments. All the experiments were carried out at ambient temperature and under similar conditions.

4.3 Results and Discussion

4.3.1 Materials characterization

The synthesized materials have been confirmed by using XRD and all peaks are well matched by using JCPDS card no. 15-0806 as cleared from **figure 4.1**.

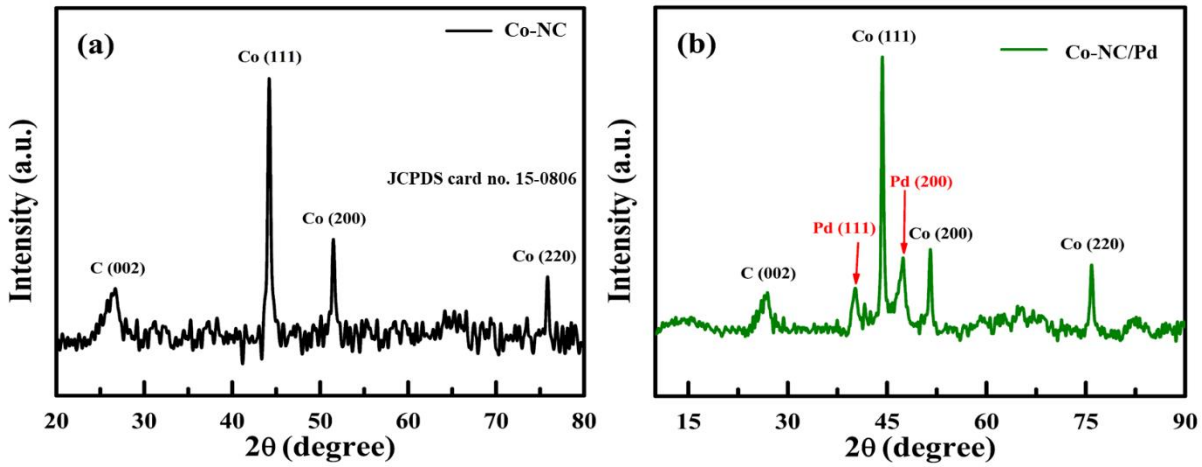

Figure 4.1 XRD spectra (a) Co-NC, (b) Co-NC/Pd

The XRD spectrum of Co-NC displays the metallic cobalt diffraction peak at 2θ values 44.20°, 51.45°, and 75.85°, which correspond to planes (111), (220), and (220), respectively [29]. Additionally, NC displays a broad peak at around ≈26.37°, which is associated with the carbon matrix's (002) peak. The Co-NC/Pd exhibits the typical palladium metal peak at 40.16° and 47.43°, which correspond to planes (111) and (200). Carbon (002) is indicated by the 2θ value at 26.71°. The (111), (200), and (220) planes of metallic cobalt are displayed at peaks at 44.35°, 51.51°, and 75.95°, as shown in **figure 4.1(a, b)**.

To learn more specifically about the states of cobalt, nitrogen, palladium, carbon, at the surface of the catalysts, XPS investigation for Co-NC/Pd nanocomposite samples has been carried out.

The different Co-species are present, as shown in **figure 4.2 (a)** by the deconvolution of Co 2p peaks. Co^{2+} ($2p^{3/2}$) species are represented by the peak at 780.75 eV, whereas metallic cobalt (Co $2p^{3/2}$) is represented by the peak at 778.75 eV, and Co^{2+} ($2p^{1/2}$) species are revealed by the peak at 796.55 eV, while the peak around 793.8 eV represents the metallic cobalt (Co $2p^{1/2}$) [30].

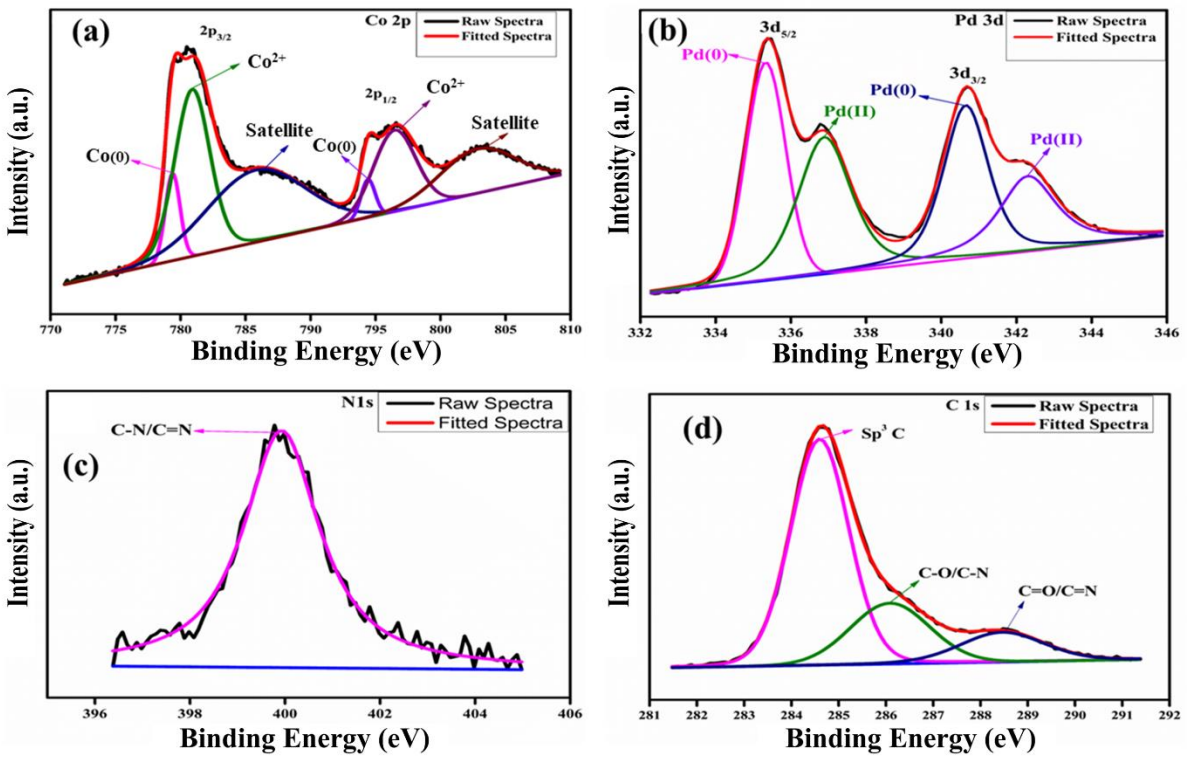

Figure 4.2 XPS analysis of Co-NC/Pd nanocomposite (a) Co 2p, (b) Pd 3d, (c) N 1s, and (d) C 1s spectrum.

Figure 4.2(b) represents the XPS spectrum of Pd in which the peaks in the spectra are deconvoluted in four peaks having binding energy around 341 eV, 342.2 eV, 335.5 eV, and 336.88 eV, respectively, corresponding to $3d^{3/2}$ and $3d^{5/2}$. The binding energy around 341 eV and 342.2 eV reveals metallic palladium and Pd^{2+} correspond to $3d^{3/2}$, whereas 335.5 eV and 336.88 eV correspond to $3d^{5/2}$, respectively [31]. The binding energy peak around 399.95 eV demonstrated the C−N/C=N as revealed in **figure 4.2 (c)** [32]. According to **figure 4.2 (d)**, the

high-resolution C 1s shows three different C species, including C-C (284.6 eV), C−N (285.9 eV), and C=N & C=O (288.6 eV) [33,34].

The microstructure and properties of the synthesized materials at the nanoscale were examined using the techniques of transmission electron microscopy (TEM) and scanning electron microscopy (SEM). SEM image as revealed in **figure 4.3 (a, b)** as prepared Co-NTA looks like non-homogeneous structures (rod shaped structures wrapped with spherical bodies). According to figure 4.3 (b) a number of spherical particles were created. Some particles were clearly separated from one another, but the majority were clumped together. The TEM image in **figure 4.3 (c)** corresponds to Pd nanoparticles having particles size 7±2 nm and triangular, cube, sphere-like geometry; **figure 4.3 (d)** rod shape structure of Co-NTA, figure 4.3(e) rod and sphere-like structure of Co-NC, having their average particles size 40±5 nm and **figure 4.2 (f)** non-homogeneous structure of Co-NC/Pd nanoparticles. It is observed from figure 4.3 (f) that Pd nanoparticles stacked on the Co-NC nanoparticles.

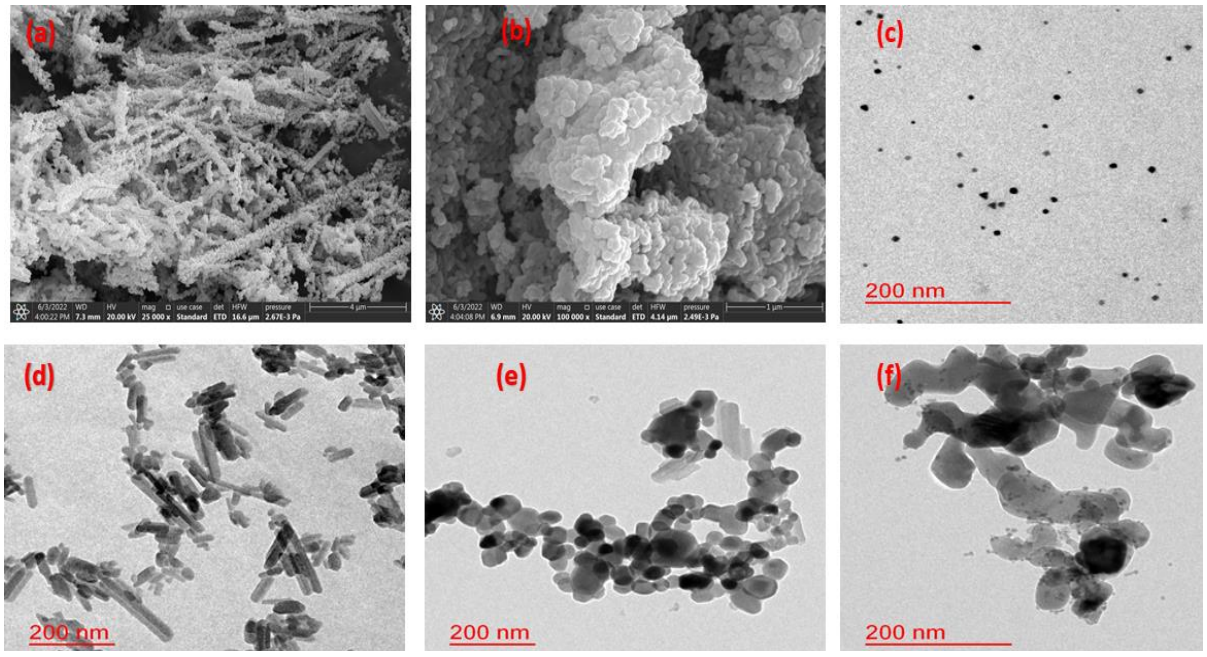

Figure 4.3 SEM images of (a) Co-NTA, (b) Co-NC, and TEM images of (c) Pd NPs, (d) Co-NTA, (e) Co-NC, and (f) Co-NC/Pd, respectively.

In **figure 4.4 (a, b)**, the EDX spectra are displayed which confirmed the presence of all constituent elements, N, C, Co, and Si, C, N, Co, Pd in the synthesized Co-NC and Co-NC/Pd nanoparticles, respectively.

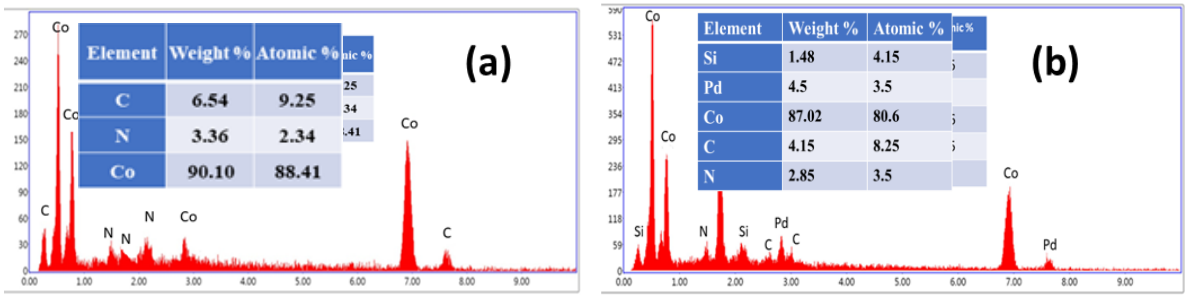

Figure. 4.4 EDX analysis for (a) Co-NC and, (b) Co-NC-Pd nanomaterials.

The SAED patterns and the calculated particle size histograms are shown in **figure 4.5.** Co-NC and Pd nanostructures of different shapes and sizes provide an opportunity to explore properties like plasmonic, electrical, and catalytic as well as their applications in biomolecule sensing [35–37]. Pd nanoparticles within Co-N doped carbon were used as a modified electrochemical sensor for the detection of NADH.

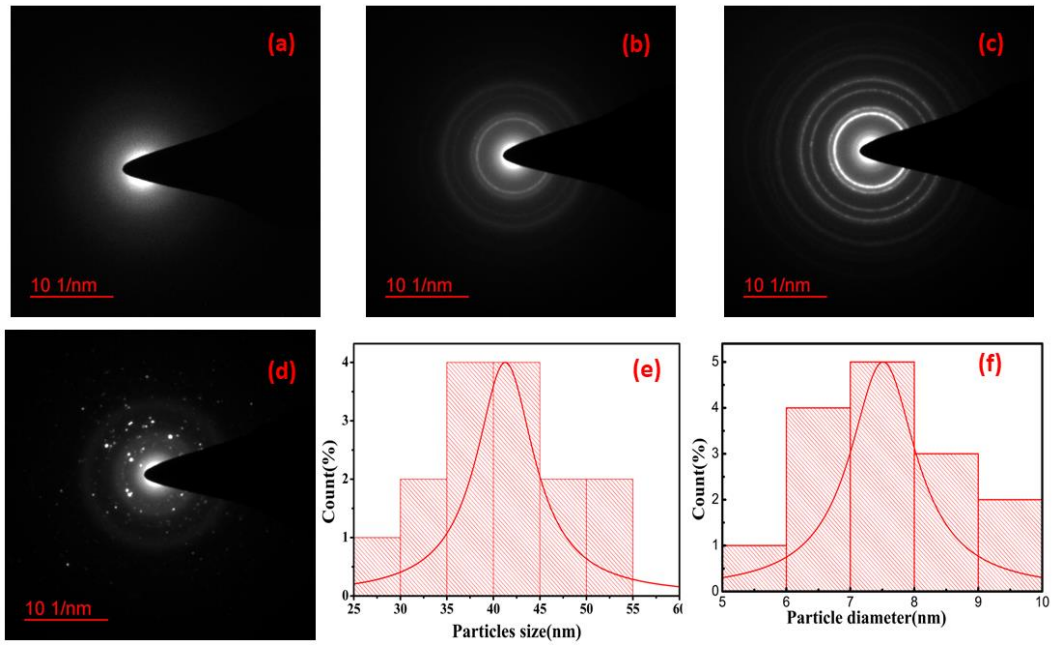

Figure 4.5 SAED patterns (a) Co-NTA, (b) Co-NC, (c) Pd nanoparticles, (d) Co-NC/Pd and Histograms (e) Co-NC, (f) Pd nanoparticles, respectively.

4.3.2 Electrochemical studies

To study the effect of Co-NC/Pd on Dmfc towards NADH sensing electrochemical study were performed. Analysis of the effect of scan rates on peak current was carried out by recording cyclic voltammograms at different scan rates starting at 0.01 Vs^{-1} to 0.5 Vs^{-1}. Co-NC/Pd/Dmfc modified electrode was built in to facilitate the electron transfer between catalytic active surface and analytes for NADH sensing. The electrochemical behavior of the modified electrodes was examined in the absence and presence of NADH as shown in **figure 4.6**. The Co-NC/Pd/Dmfc displayed enhanced electrocatalytic activities in the presence of NADH compared to the absence of NADH, suggesting that the Co-Pd nanocomposite catalyst could be a promising material for NADH sensing. The modified electrode with Co-NC/Pd revealed better redox behavior and high current response as it can be seen from **figure 4.6 (a, b, c)**. The cyclic voltammetric response before and after NADH addition has been examined and found through the use of electron transfer mediation, the change in peak potential and the increased current signal can be explained as a catalytic effect as revealed in **figure 4.6 (d, e, f)**.

As shown in **figure 4.6**, the modified electrode Dmfc/Co-NC/Pd caused the NADH oxidation peak potential to shift in a more positive direction, confirming the electrochemical irreversibility of the process, which can be clearly seen in **figure 4.7** [38–40].

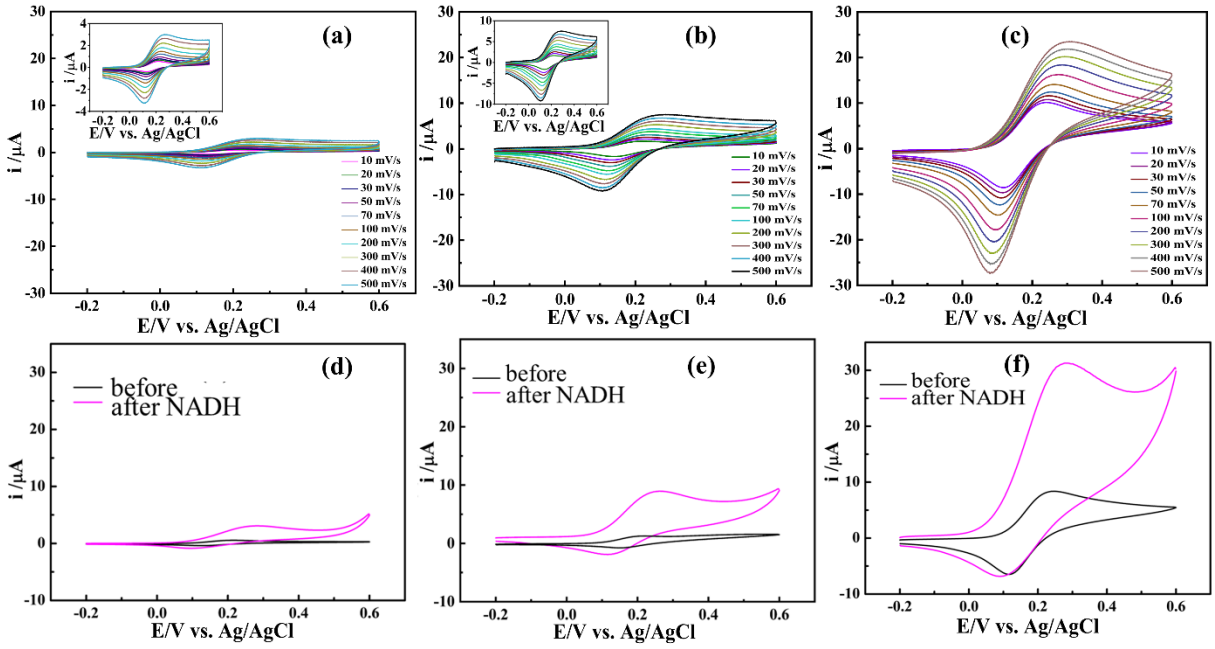

Figure 4.6 Cyclic voltammetric study before the addition NADH (a) Dmfc, (b) Dmfc-Co-NC, (c) Dmfc-Co-NC/Pd at various scan rates (10 to 500 mV/s) and after the addition of NADH (5 mM) (d), (e), and (f) at 10 mV/s, respectively under similar condition. Inset figure is used for clear visibility of cycle.

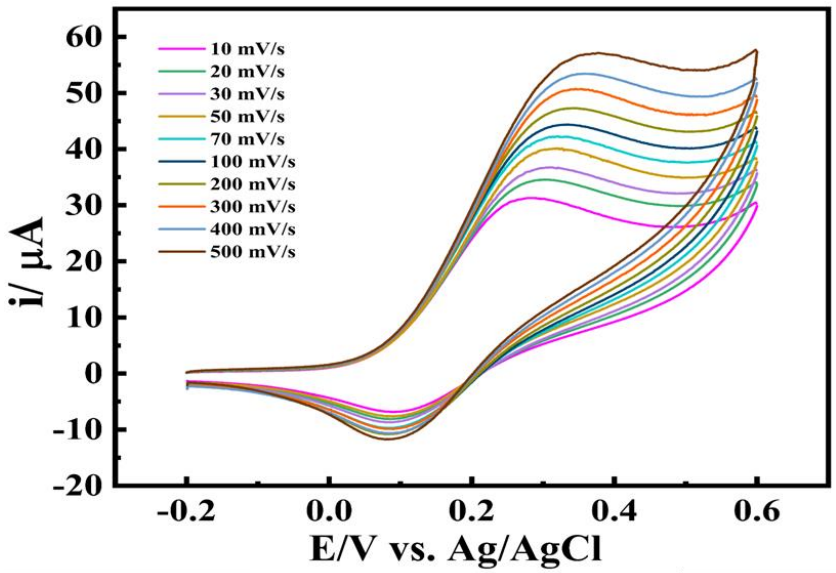

Figure 4.7 Cyclic voltammetric response with Dmfc/Co-NC/Pd modified electrode after NADH addition.

The data has been correlated with Randles-Sevcik equation and the reaction was found to be diffusion controlled. The Randles-Sevcik equation, $I_p = 2.69 \times 10^5 D^{1/2} A C \sqrt{v} n^{3/2}$

Where I_p peak current, A is the surface area of electrodes (cm^2), C is the concentration (mol/L), ν is the scan rate (Vs^{-1}), n is the number of electrons involved in a redox reaction, and D is the diffusion coefficient (cm^2/s).

The electroactive surface area was also calculated by using the following equation

$$EASA = R_f * S$$

Where R_f is the roughness factor, and S is the geometrical surface area of the electrode.

As a result, after calculating the values for R_f and S we could able to calculate an approximate value of EASA. It was found that Dmfc/CPE, Dmfc-Co-NC/CPE, and Dmfc-Co-NC/Pd/CPE have electroactive surfaces of 0.210 cm^2, 0.258 cm^2, and 0.838 cm^2, respectively. This increase in electroactive surface area can enhance the sensitivity and selectivity of modified electrodes, making them more effective in the detection of NADH. According to **figure 4.8**, the oxidation process appears to be controlled by diffusion rather than surface because the oxidation peak current grows linearly with the square root of the scan rate.

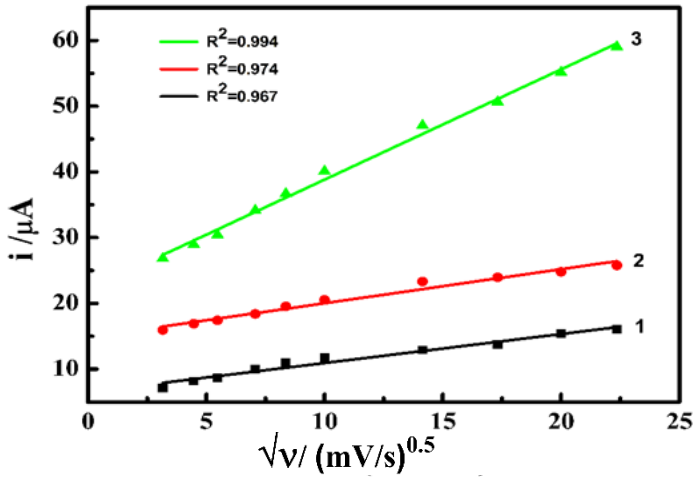

Figure 4.8 Plot of current vs square root of scan rate obtained from electrocatalytic oxidation of NADH at various scan rates using modified electrodes (1) Dmfc, (2) Dmfc/Co-NC, (3) Dmfc/Co-NC/Pd in working electrolyte at pH 7.0.

4.3.3 Electrochemical impedance study of the modified electrode

In order to learn more about the characteristics of electrodes and get specific information about charge transfer resistance, diffusion processes, and equivalent circuit fittings at the electrode/electrolyte interface, electrochemical impedance spectroscopy (EIS) is a potent technique [41,42]. Electrochemical impedance spectroscopy was performed in 0.1 M PBS (0.5 M KCl supporting electrolyte) at 0.22 V potential in the frequency range between 10 Hz to 100 kHz. The impedance (resistance and reactance) of the sample is displayed as a function of frequency on a Nyquist plot. Nyquist plot have two parts one is semicircle at higher frequency and second is linear portion towards lower frequency region. The linear part shows the diffusion-controlled process and the semicircle part reveals the charge transfer process. The outcome demonstrated that the modified electrode has outperformed than unmodified electrodes in terms of electrochemical performance, as well as low impedance and fast charge transfer as shown in **figure 4.9.**

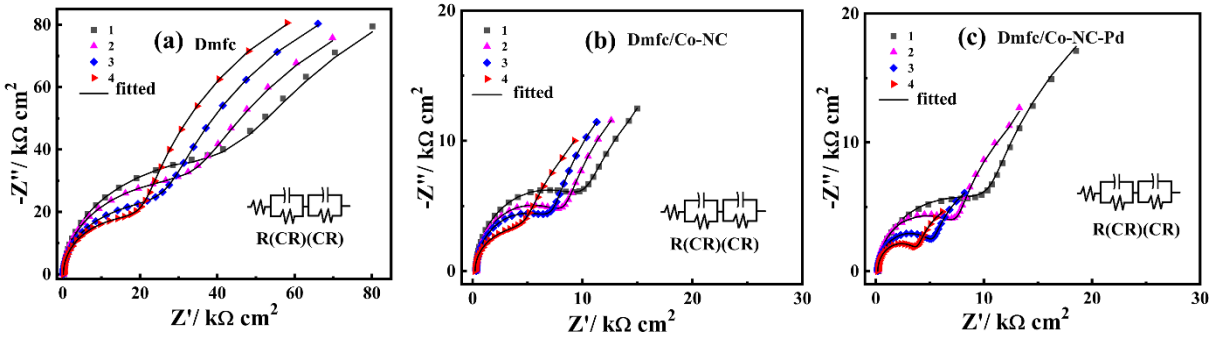

Figure 4.9 Electrochemical impedance spectroscopy (EIS) Nyquist plots using various modified electrodes **(a)** Dmfc, **(b)** Dmfc Co-NC, **(c)** Dmfc Co-NC/Pd, with a freshly prepared working electrolyte, and vary concentration of NADH (1) Blank, (2) 2.5 mM, (3) 5 mM,4) 7.5 mM

The spectra were best fitted using the extended Randles equivalent circuit R(CR)(CR). The Nyquist plot's circle component's diameter suggests that the Dmfc/Co-NC/Pd modified electrode has better catalytic performance and higher charge transfer rate than the unmodified

Dmfc electrode and that the Dmfc-Co-NC modified electrode. R_{ct} which is equal to its diameter, reveals the conductivity and governed the electrons transfer kinetics at the electrode surface [38,43]. The calculated charge transfer resistance (R_{ct}) value is shown in Table 4.2. Furthermore, as the NADH concentration increases, the circle's diameter decreases and the charge transfer process gradually accelerates.

Table 4.2 Table for charge transfer resistance **(R_{ct})** for the modified electrodes

Concentration of NADH	Dmfc R_{ct} (kΩ cm^2)	Dmfc/Co-NC R_{ct} (kΩ cm^2)	Dmfc/Co-NC/Pd R_{ct} (kΩ cm^2)
Blank	62.22	14.54	12.50
2.5 mM	53.38	11.50	7.44
5.0 mM	37.40	8.82	5.17
7.5 mM	27.46	6.15	3.71

4.3.4 Amperometric response of NADH using modified electrode

The observed amperometric current response during the electrooxidation of NADH by Dmfc modified electrode can be attributed to the electron transfer procedure involved in the oxidation of NADH. According to the widely accepted Electron Transfer-Chemical Reaction-Electron Transfer (ECE) mechanism, which was proposed in earlier studies [44], NADH electrooxidation occurs when electrons are transferred between chemical reactions. There were three steps involved in the mechanism.

$$NADH - e^- \longrightarrow NADH^{\cdot +} \quad \textbf{(i)}$$

$$NADH^{\cdot +} \xrightarrow{-H^+} NAD^{\cdot} \quad \textbf{(ii)}$$

$$NAD^{\cdot} \longrightarrow NAD^+ + e^- \quad \textbf{(iii)}$$

In step first the cation radical is produced as a result of de-electronation, the second step involved the irreversible oxidation of NADH resulting in the formation of the neutral NAD radical with the loss of one proton and immediately, $NAD^{\cdot}$ radical is transformed into NAD^{+} at the electrode surface. The Modified electrode Co-NC/Pd-Dmfc shows superior electrochemical behavior and high current during the i-t curve study. The current response has been seen to increase in a stable, linear step-up-wise fashion from the amperometric i-t curves. The calibration curve shows the linear response between 5 µM to 1250 µM and the lowest detection limit of 2 µM as shown in **figure 4.10.**

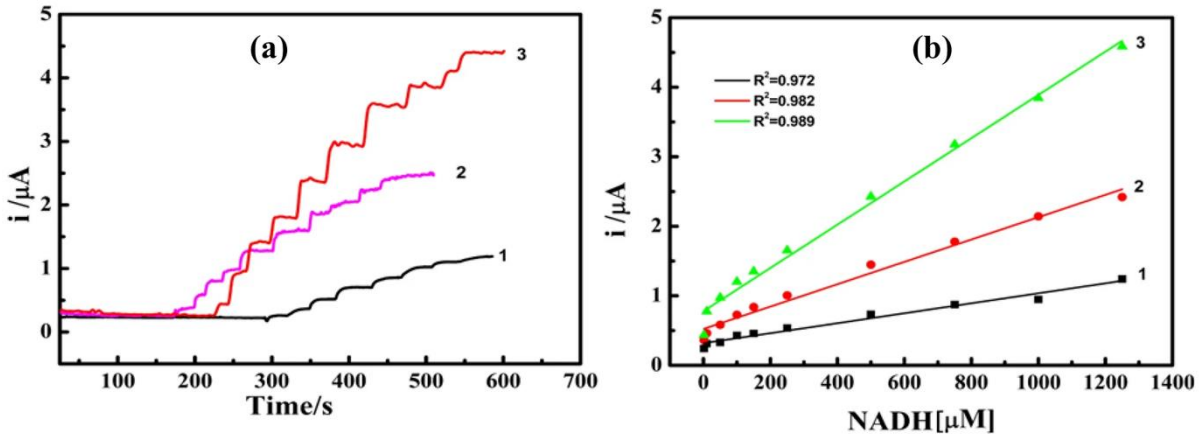

Figure 4.10 (a) Amperometric response of NADH (2-1250 µM) with 5 µL of successive addition in 0.1 M PBS (containing 0.5 M KCl) at the applied potential at 0.22 V, (1) Dmfc, (2) Dmfc-Co-NC, (3) Dmfc-Co-NC/Pd and (b) Calibration curve, current vs concentration obtained from amperometric i-t curves.

The sensitivity of carbon paste modified electrode Dmfc, Co-NC Dmfc, and Co-NC-Pd/Dmfc electrodes for NADH sensing was observed to be 0.097, 1.94, and 3.69 µA/mM, respectively, confirming that the modified electrode has high sensitivity due to palladium and its nano geometry on electroanalysis. The analytical outcomes were compared to data from the previously published literature on the electroanalytical detection of NADH at different modified electrodes (Table 4.3). It is noticeable that such values obtained for other systems are equivalent to the LOD and linear range.

Table 4.3 The comparative table of the efficiency of various analytical techniques for the detection of NADH

Method	Modified electrode/material	LOD (µM)	Linear range (µM)	Reference
Fluorescence	Ag nanocluster	22.30	50-500	[45]
Absorption	Au nanorods	4.03	4.03-49	[2]
Amperometry	PEDOT CMs/GCE	5.30	20-240	[46]
Amperometry	PTZ/AgRNPs/SPE	0.52	1.9-89	[21]
Electrochemistry	SPCE/MWCNT/AuNP	3.72	12.4-150	[47]
Chronoamperometry	AuNR@rGO/GCE	0.22	1-31	[48]
Amperometry	NPG/SPE	16.00	50 µM-2 mM	[40]
Amperometry	**Co-NC/Pd/Dmfc**	**2.00**	**5-1250**	**This work**

PEDOT cms- Poly(ethylenedioxythiophene) colloidal microparticles, PTZ- phenothiazine, SPCE- screen-printed carbon electrodes, GCE-glassy carbon electrodes, rGO-reduced graphene oxide

4.3.5 Effect of pH and Scan rate

We looked at how pH changed across a broad pH range in terms of the amperometric response current of NADH. Our findings showed in **figure 4.11**, that the amperometric current increased as pH rise, reaching its peak activity at pH 7.0. At this point, further, decrease results in a steady state with a peak current that reverses its decline at pH 9. As a result, pH 7.0 was identified as the ideal working pH value. The influence of scan rate, another crucial electrochemical parameter, may also have an impact on the speed of electron transfer and the sensitivity of the detection. In order to study the oxidation peak currents of a single concentration of NADH, several scan rates were used.

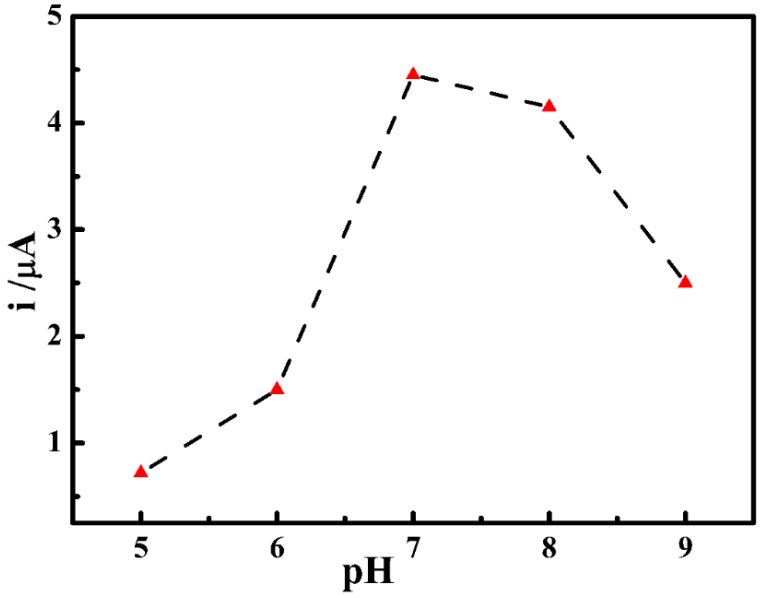

Figure 4.11 Effect of pH on amperometric response current of NADH using Dmfc/Co-Pd-NC modified electrode.

As a consequence, graphs of the oxidation peak current vs the square root of the scan rate were created using the Randles-Sevcik principle [49]. Our findings, which are represented in figure 4.8, demonstrated that the peak current increased linearly as a function of the square root of the scan rate, supporting the notion that the electrochemical reaction is a diffusion-controlled process.

4.3.6 Stability and Reproducibility

The most important criteria for assessing the efficiency and use of any constructed sensors are stability and reproducibility. Amperometry was used in this instance to assess the operational stability of the created modified electrodes under dynamic circumstances. Amperometric i-t responses were observed at Dmfc/Co-NC/Pd modified electrodes under working electrolyte with 20 mM NADH present and absent at an applied potential of +0.22 V is revealed in **figure 4.12 (a)**. There were no obvious alterations in the lack of NADH at Dmfc/Co-NC/Pd modified

electrode even after 600 s. Although there was a minor drop or insignificant drop (less than 1%) in the catalytic current when NADH was present [50].

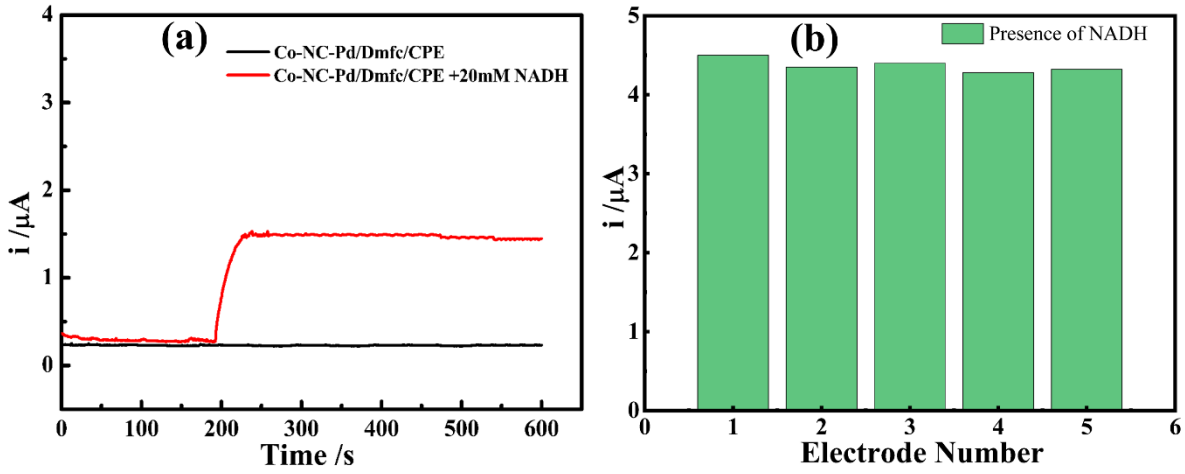

Figure 4.12 Amperometric i-t response of (a) Dmfc/Co-NC/Pd carbon paste electrode in the absence and presence of 20 mM NADH at +0.22 V for 600 s under constant stirring, (b) Amperometric response of 1.25 mM NADH is illustrated by the current response columnar diagram of five separately made Dmfc-Co-NC/Pd modified electrodes.

Also, by building five modified electrodes independently and employing them for the electrocatalytic analysis of NADH, the reproducibility of the created sensor was examined. The created sensor's great reproducibility is demonstrated by the columnar diagram of the current response produced for the independently constructed Dmfc/Co-NC-Pd modified electrode towards 1.25 mM NADH measurement, which, as shown in **figure 4.12 (b)**, has a relative standard deviation (%RSD) of 1.94%.

4.4 Conclusions

The catalytic performance of the sensor made with mediated Dmfc-Co-NC/Pd has been improved drastically when it comes to oxidizing NADH. For the electrocatalytic oxidation of NADH, Co-NC/Pd was used to modify the electrode surface with a suitable mediator, Dmfc. With a linear response between 5 µM and 1250 µM (R^2=0.989) and a sensitivity of 3.69

μA/mM, the Co-NC/Pd /Dmfc electrodes demonstrate good analytical performance for the detection of NADH. This electrochemical sensor has been demonstrated to be extremely sensitive and accurate for detecting NADH in working electrolyte. One of the main elements of the upcoming sensor generation is reliable and producible catalytic electrodes for NADH oxidation.

4.5 References

[1] M. Shivakumar, S. Manjunatha, M.S. Dharmaprakash, S.B. M, Biological activity of PdNPs derived from hemicellulose via microwave assisted green synthesis, *Curr*. *Res*. *Green Sustain*. *Chem*., **4** (2021): 100150. https://doi.org/10.1016/j.crgsc.2021.100150.

[2] G. Weng, X. Zhao, J. Zhao, J. Li, J. Zhu, J. Zhao, Nanoplasmonic sensing of NADH by inhibiting the oxidative etching of gold nanorods, *Sens*. *Actuators B*: *Chem*., **299** (2019): 126982. https://doi.org/10.1016/j.snb.2019.126982.

[3] S. Immanuel, R. Sivasubramanian, Electrochemical kinetic investigation of NADH oxidation on Prussian blue-mediated chemically reduced graphene oxide nanosheets, *J*. *Phys*. *Chem*. *Solids*, **161** (2022): 110471. https://doi.org/10.1016/j.jpcs.2021.110471.

[4] L. Wang, J. Zhang, B. Kim, J. Peng, S.N. Berry, Y. Ni, D. Su, J. Lee, L. Yuan, Y.-T. Chang, Boronic Acid: A Bio-Inspired strategy to increase the sensitivity and selectivity of fluorescent NADH probe, *J*. *Am*. *Chem*. *Soc*., **138**, no. 33 (2016): 10394-10397. https://doi.org/10.1021/jacs.6b05810.

[5] P. Manusha, S. Senthilkumar, Development of a ferrocene-tethered ionic liquid modified electrode for non-enzymatic electrochemical sensing of NADH, *J*. *Mater*. *Sci*.: *Mater*. *Electron*., **33** (2022): 8576–8585. https://doi.org/10.1007/s10854-021-06576-0.

[6] N.F. Atta, S.A. Abdel Gawad, E.H. El-Ads, A.R.M. El-Gohary, A. Galal, A new strategy for NADH sensing using ionic liquid crystals-carbon nanotubes/nano-magnetite composite platform, *Sens*. *Actuators* B: *Chem*., **251** (2017): 65–73. https://doi.org/10.1016/j.snb.2017.05.026.

[7] Y. Mie, Y. Yasutake, M. Ikegami, T. Tamura, Anodized gold surface enables mediator-free and low-overpotential electrochemical oxidation of NADH: A facile method for the development of an NAD^+-dependent enzyme biosensor, *Sens*. *Actuators* B: *Chem*., **288** (2019): 512–518. https://doi.org/10.1016/j.snb.2019.03.039.

[8] W. Xie, A. Xu, E.S. Yeung, Determination of NAD^+ and NADH in a single cell under hydrogen peroxide stress by capillary electrophoresis, *Anal*. *Chem*., **81** (2009): 1280–1284. https://doi.org/10.1021/ac802249m.

[9] M. Chu, Z. Bai, D. Zhu, W. Chen, G. Yang, J. Xin, H. Ma, H. Pang, L. Tan, X. Wang, A β-nicotinamide adenine dinucleotide electrochemical sensor based on polyoxometalate built by the combination of electrodeposition and self-assembly, *J*. *Electroanal*. *Chem*., **907** (2022): 116083. https://doi.org/10.1016/j.jelechem.2022.116083.

[10] M. Wang, X. Kan, Multilayer sensing platform: gold nanoparticles/prussian blue decorated graphite paper for NADH and H_2O_2 detection, *Analyst*, **143** (2018): 5278–5284. https://doi.org/10.1039/c8an01502c.

[11] K.K. Maurya, K. Singh, M. Malviya, Effect of palladium and its nanogeometry on the redox electrochemistry of tetracyanoquinodimethane modified electrode; application in electrochemical sensing of ascorbic acid, *J*. *Appl*. *Electrochem*., (9) **53** (2023): 1831-1842. https://doi.org/10.1007/s10800-023-01878-z.

[12] A.S. Agnihotri, A. Varghese, N. M, Transition metal oxides in electrochemical and bio sensing: A state-of-art review, *Appl*. *Surf*. *Sci*. *Adv*., **4** (2021): 100072. https://doi.org/10.1016/j.apsadv.2021.100072.

[13] J.M. George, A. Antony, B. Mathew, Metal oxide nanoparticles in electrochemical sensing and biosensing: a review, *Microchim*. *Acta*, **185** (2018): 1-26. https://doi.org/10.1007/s00604-018-2894-3.

[14] P. Liang, H. Yu, B. Guntupalli, Y. Xiao, Paper-based device for rapid visualization of NADH based on dissolution of gold nanoparticles, *ACS Appl*. *Mater*. *Interfaces*, **7** (2015): 15023–15030. https://doi.org/10.1021/acsami.5b04104.

[15] H. Jaegfeldt, T. Kuwana, G. Johanssont, Electrochemical Stability of Catechols with a Pyrene Side Chain Strongly Adsorbed on Graphite Electrodes for Catalytic Oxidation of Dihydronicotinamide Adenine Dinucleotide, *J*. *Am*. *Chem*. *Soc*., (7) **105** (1983):1805-1814. https://doi.org/10.1021/ja00345a021

[16] G.P. Keeley, A. O'Neill, M. Holzinger, S. Cosnier, J.N. Coleman, G.S. Duesberg, DMF-exfoliated graphene for electrochemical NADH detection, *Phys*. *Chem*. *Chem*. *Phys*., **13** (2011): 7747–7750. https://doi.org/10.1039/c1cp20060g.

[17] C. Shan, H. Yang, D. Han, Q. Zhang, A. Ivaska, L. Niu, Electrochemical determination of NADH and ethanol based on ionic liquid-functionalized graphene, *Biosens*. *Bioelectron*., **25** (2010): 1504–1508. https://doi.org/10.1016/j.bios.2009.11.009.

[18] Y. Liu, R. Landick, S. Raman, A Regulatory NADH/NAD^+ Redox Biosensor for Bacteria, *ACS Synth*. *Biol*., **8** (2019): 264–273. https://doi.org/10.1021/acssynbio.8b00485.

[19] R.D. Nagarajan, P. Murugan, A.K. Sundramoorthy, Selective Electrochemical Sensing of NADH and NAD^+ Using Graphene/Tungstate Nanocomposite Modified Electrode, *ChemistrySelec*t, **5** (2020): 14643–14651. https://doi.org/10.1002/slct.202003554.

[20] A. Koyappayil, H.T. Kim, M.H. Lee, An efficient and rapid synthesis route to highly fluorescent copper microspheres for the selective and sensitive excitation wavelength-dependent dual-mode sensing of NADH, *Sens*. *Actuators* B: *Chem*., **327** (2021): 128887. https://doi.org/10.1016/j.snb.2020.128887.

[21] P. Manusha, S. Yadav, J. Satija, S. Senthilkumar, Designing electrochemical NADH sensor using silver nanoparticles/phenothiazine nanohybrid and investigation on the shape dependent sensing behavior, *Sens*. *Actuators* B: *Chem*., **347** (2021):130649. https://doi.org/10.1016/j.snb.2021.130649.

[22] L. Zhu, R. Yang, X. Jiang, D. Yang, Amperometric determination of NADH at a Nile blue/ordered mesoporous carbon composite electrode, *Electrochem*. *Commun*., **11** (2009): 530–533. https://doi.org/10.1016/j.elecom.2008.12.045.

[23] S. Shahrokhian, R. Salimian, S. Rastgar, Pd-Au nanoparticle decorated carbon nanotube as a sensing layer on the surface of glassy carbon electrode for electrochemical determination of ceftazidime, *Mater*. *Sci*. *Eng*. *C*, **34** (2014): 318–325. https://doi.org/10.1016/j.msec.2013.09.014.

[24] G. Maduraiveeran, R. Ramaraj, Silver nanoparticles embedded in amine-functionalized silicate sol-gel network assembly for sensing cysteine, adenosine and NADH, *J*. *Nanoparticle Res*., **13** (2011): 4267–4276. https://doi.org/10.1007/s11051-011-0372-5.

[25] X.H. Pham, C.A. Li, K.N. Han, B.C. Huynh-Nguyen, T.H. Le, E. Ko, J.H. Kim, G.H. Seong, Electrochemical detection of nitrite using urchin-like palladium nanostructures on carbon nanotube thin film electrodes, *Sens*. *Actuators* B: *Chem*., **193** (2014): 815–822. https://doi.org/10.1016/j.snb.2013.12.034.

[26] S.H. Lim, J. Wei, J. Lin, Q. Li, J. KuaYou, A glucose biosensor based on electrodeposition of palladium nanoparticles and glucose oxidase onto Nafion-solubilized carbon nanotube electrode, *Biosens. Bioelectron.*, **20** (2005): 2341–2346. https://doi.org/10.1016/j.bios.2004.08.005.

[27] B. Singh, N. Bhardwaj, V.K. Jain, V. Bhatia, Palladium nanoparticles decorated electrostatically functionalized MWCNTs as a non-enzymatic glucose sensor, *Sens. Actuators A: Phys.*, **220** (2014): 126–133. https://doi.org/10.1016/j.sna.2014.09.030.

[28] B. Wang, K. Chen, G. Wang, X. Liu, H. Wang, J. Bai, A multidimensional and hierarchical carbon-confined cobalt phosphide nanocomposite as an advanced anode for lithium and sodium storage, *Nanoscale*, **11** (2019): 968–985. https://doi.org/10.1039/c8nr07076h.

[29] G. Zhang, L. Liu, Q. Zhu, X. Kong, Chemoselective Hydrogenation of Nitroarenes by an Efficient Co@NC/AC Catalyst, *Catal. Letters*, **153** (2023): 1536–1542. https://doi.org/10.1007/s10562-022-04085-1.

[30] K. Murugesan, T. Senthamarai, A.S. Alshammari, R.M. Altamimi, C. Kreyenschulte, M.M. Pohl, H. Lund, R. V. Jagadeesh, M. Beller, Cobalt-Nanoparticles Catalyzed Efficient and Selective Hydrogenation of Aromatic Hydrocarbons, *ACS Catal.*, **9** (2019): 8581–8591. https://doi.org/10.1021/acscatal.9b02193.

[31] W. Yi, Z. Li, C. Dong, H.W. Li, J. Li, Electrochemical detection of chloramphenicol using palladium nanoparticles decorated reduced graphene oxide, *Microchem. J.* **148** (2019): 774–783. https://doi.org/10.1016/j.microc.2019.05.049.

[32] R. Zhang, M. Tahir, S. Ding, M.A. Qadeer, H. Li, Q.X. Zeng, R. Gao, L. Wang, X. Zhang, L. Pan, J.J. Zou, Promotion of Nitrogen Reserve and Electronic Regulation in Bamboo-like Carbon Tubules by Cobalt Nanoparticles for Highly Efficient ORR, *ACS Appl. Energy Mater.*, **3** (2020): 2323–2330. https://doi.org/10.1021/acsaem.9b01617.

[33] K. Zhu, C. Jin, Z. Klencsár, A.S. Ganeshraja, J. Wang, Cobalt-iron oxide, alloy and nitride: Synthesis, characterization and application in catalytic peroxymonosulfate activation for orange II degradation, *Catalysts*, **7** (2017): 138. https://doi.org/10.3390/catal7050138.

[34] S. Liang, C. Liang, High-density cobalt nanoparticles encapsulated with nitrogen-doped carbon nanoshells as a bifunctional catalyst for rechargeable zinc-air battery, *Materials*, **12** (2019): 243. https://doi.org/10.3390/ma12020243.

[35] A. Chen, C. Ostrom, Palladium-Based Nanomaterials: Synthesis and Electrochemical Applications, *Chem*. *Rev*., **115** (2015): 11999–12044. https://doi.org/10.1021/acs.chemrev.5b00324.

[36] Y. Xiong, Y. Xia, Shape-controlled synthesis of metal nanostructures: The case of palladium, *Adv*. *Mater*., **19** (2007): 3385–3391. https://doi.org/10.1002/adma.200701301.

[37] K. Białas, D. Moschou, F. Marken, P. Estrela, Electrochemical sensors based on metal nanoparticles with biocatalytic activity, *Microchim*. *Acta*, **189** (2022): 172. https://doi.org/10.1007/s00604-022-05252-2.

[38] B. Fall, D.D. Sall, M. Hémadi, A.K.D. Diaw, M. Fall, H. Randriamahazaka, S. Thomas, Highly efficient non-enzymatic electrochemical glucose sensor based on carbon nanotubes functionalized by molybdenum disulfide and decorated with nickel nanoparticles (GCE/CNT/MoS_2/NiNPs), *Sens*. *Actuators Rep*. **5** (2023): 100136. https://doi.org/10.1016/j.snr.2022.100136.

[39] H. Elsawy, B.M. Thamer, A. Sedky, M.H. El-Newehy, Facile two-step synthesis of nickel nanoparticles supported on 3D porous carbon frameworks as an effective electrocatalyst for urea and methanol oxidation, *Mater*. *Chem*. *Phys*., **297** (2023): 127361. https://doi.org/10.1016/j.matchemphys.2023.127361.

[40] S. Chen, K. Shang, X. Gao, X. Wang, The development of NAD^+-dependent dehydrogenase screen-printed biosensor based on enzyme and nanoporous gold co-catalytic strategy, *Biosens*. *Bioelectron*., **211** (2022): 114376. https://doi.org/10.1016/j.bios.2022.114376.

[41] T. Anusha, K.S. Bhavani, J. V. Shanmukha Kumar, P.K. Brahman, R.Y.A. Hassan, Fabrication of electrochemical immunosensor based on GCN-β-CD/Au nanocomposite for the monitoring of vitamin D deficiency, *Bioelectrochemistry*, **143** (2022): 107935. https://doi.org/10.1016/j.bioelechem.2021.107935.

[42] H.S. Magar, R.Y.A. Hassan, A. Mulchandani, Electrochemical impedance spectroscopy (EIS): Principles, construction, and biosensing applications, *Sensors*, **21** (2021): 6578. https://doi.org/10.3390/s21196578.

[43] R. Aghajari, A. Azadbakht, Amplified detection of streptomycin using aptamer-conjugated palladium nanoparticles decorated on chitosan-carbon nanotube, *Anal*. *Biochem*., **547** (2018): 57–65. https://doi.org/10.1016/j.ab.2018.02.005.

[44] C.E. Banks, R.G. Compton, Exploring the electrocatalytic sites of carbon nanotubes for NADH detection: An edge plane pyrolytic graphite electrode study, *Analyst*, **130** (2005): 1232–1239. https://doi.org/10.1039/b508702c.

[45] P. Jain, B. Chakma, S. Patra, P. Goswami, Hairpin stabilized fluorescent silver nanoclusters for quantitative detection of NAD^+ and monitoring NAD^+/NADH based enzymatic reactions, *Anal*. *Chim*. *Acta*, **956** (2017): 48–56. https://doi.org/10.1016/j.aca.2016.12.030.

[46] L. Meng, A.P.F. Turner, W.C. Mak, Positively-charged hierarchical PEDOT interface with enhanced electrode kinetics for NADH-based biosensors, *Biosens*. *Bioelectron*., **120** (2018): 115–121. https://doi.org/10.1016/j.bios.2018.08.017.

[47] M. Sahin, E. Ayranci, Electrooxidation of NADH on Modified Screen-Printed Electrodes: Effects of Conducting Polymer and Nanomaterials, *Electrochim*. *Acta*, **166** (2015): 261–270. https://doi.org/10.1016/j.electacta.2015.03.030.

[48] A.R. Marlinda, S. Sagadevan, N. Yusoff, A. Pandikumar, N.M. Huang, O. Akbarzadeh, M.R. Johan, Gold nanorods-coated reduced graphene oxide as a modified electrode for the electrochemical sensory detection of NADH, *J*. *Alloys Compd*., **847** (2020): 156552. https://doi.org/10.1016/j.jallcom.2020.156552.

[49] S.N. Prashanth, K.C. Ramesh, J. Seetharamappa, Electrochemical Oxidation of an Immunosuppressant, Mycophenolate Mofetil, and Its Assay in Pharmaceutical Formulations, *Int*. *J*. *Electrochem*., **2011** (2011): 1–7. https://doi.org/10.4061/2011/193041.

[50] M. Elancheziyan, K. Theyagarajan, V.K. Ponnusamy, K. Thenmozhi, S. Senthilkumar, Porous graphene oxide based disposable non-enzymatic electrochemical sensor for the determination of nicotinamide adenine dinucleotide, *Micro Nano Eng*., **15** (2022): 100133. https://doi.org/10.1016/j.mne.2022.100133.